PNAS RESEARCH ARTICLE | CELL BIOLOGY
APPLIED PHYSICAL SCIENCES

In situ licensing of mesenchymal stem cell immunomodulatory function via BMP-2 induced developmental process

Fuwei Zhu[a,b], Luli Ji[a,b], Kai Dai[a,b], Shunshu Deng[a,b], Jing Wang[a,b,c,1], and Changsheng Liu[b,c,d,1]

Affiliations are included on p. 12.

Edited by David Weitz, Harvard University, Cambridge, MA; received May 30, 2024; accepted October 21, 2024

The immunomodulatory function of mesenchymal stem cells (MSCs) is plastic and susceptible to resident microenvironment in vivo or inflammatory factors in vitro. We propose a unique method to enhance the immunoregulatory functions of mesenchymal stem cells (MSCs) through an artificially controllable in vivo inflammatory microenvironment generated by biomaterials loaded with BMP-2 that induce bone development. MSCs activated through this method effectively induce M1 macrophage polarization toward the M2 phenotype, promote differentiation of naïve T cells into regulatory T cells, and inhibit the proliferation of activated T cells via prostaglandin E2 (PGE2) secretion. This in vivo licensing not only preserves the immunogenicity of MSCs but also alters DNA methylation patterns, enabling MSCs to exhibit immunoregulatory effects with epigenetic memory. Validation in a mouse colitis model demonstrated their therapeutic efficacy and long-term viability. Furthermore, we found that the material composition influences the inflammatory response during development, with polysaccharide-based biomaterials proving advantageous over protein-based materials in establishing an inflammatory niche conducive to MSC activity. These findings underscore the potential of tissue engineering to create in vivo environments that license MSCs, offering a strategic avenue to enhance MSC-based therapies for addressing significant immune disorders.

mesenchymal stem cells | osteo-organoids | inflammatory | immunomodulatory | immunogenicity

Significance

Inflammatory factors, while enhancing the immunomodulatory capabilities of mesenchymal stem cells (MSCs), also upregulate the expression of cell surface histocompatibility antigens, compromising the immune privilege of MSCs. Here, we combine the biological effects of materials with the osteogenic induction capabilities of Bone Morphogenetic Protein (BMP)-2 to develop a unique method for in situ licensing of MSCs' immunomodulatory function within a controlled inflammatory microenvironment constructed in vivo. This method not only yields a large quantity of high-quality MSCs but also imparts lower immunogenicity and prolonged efficacy, presenting a different paradigm for treating immune and inflammation-related diseases.

Mesenchymal stem cells (MSCs) have attracted widespread clinical attention due to their multidirectional differentiation potential, immunomodulatory properties, anti-inflammatory effects, and low immunogenicity (1–3). In the clinical research and treatment of inflammatory diseases such as Crohn's disease, graft-versus-host disease, systemic lupus erythematosus, and organ fibrosis, MSCs have demonstrated their ability to suppress inflammation, alleviate disease progression (4–7). However, infused MSCs exhibit limited survival and differentiation in damaged tissue environments (8), suggesting that they primarily exert their effects on immune cells through a "cellular empowerment" mechanism via paracrine signaling (9). By secreting factors such as nitric oxide (NO), prostaglandin E2 (PGE2), transforming growth factor-β (TGF-β), hepatocyte growth factor (HGF), and tumor necrosis factor-inducing gene 6 protein (TSG6), MSCs modulate the recruitment, proliferation, and function of macrophages, neutrophils, NK cells, and T cells (4, 10–13). In this way, MSCs play a pivotal role in modulating inflammation and immune.

Recent studies have highlighted the plasticity of MSCs' immunomodulatory functions, showing that the inflammatory environment significantly influences their biological fate (14). Higher levels of inflammation enhance MSC efficacy in inhibiting graft-versus-host disease (GvHD), while effectiveness diminishes in low-inflammation settings, particularly early in the disease (15). Similarly, MSC therapy during the active phase of encephalomyelitis (EAE) yields better outcomes than during the recurrent phase (16). These findings suggest that MSCs are modulated by surrounding immune cells upon recruitment to inflammatory sites. Their immunomodulatory functions are activated by cytokines in the inflammatory milieu, leading researchers to pretreat MSCs with inflammatory factors to enhance their immunoregulatory capabilities (17, 18). However, this pretreatment method can induce the expression of major histocompatibility complex class II (MHC-II) on MSCs, resulting in lost immune privilege and faster clearance by the host's immune system, ultimately diminishing therapeutic efficacy (19, 20). Additionally, the enhancements in MSCs' function following pretreatment are transient, as their immunosuppressive ability declines with prolonged in vitro culture time (21, 22). These limitations restrict the clinical application of pretreating MSCs with inflammatory factors.

To develop a unique licensing method that enhances the clinical efficacy of MSCs by activating their immunomodulatory capabilities of MSCs while avoiding the side effects

Author contributions: F.Z., J.W., and C.L. designed research; F.Z. and L.J. performed research; F.Z., L.J., K.D., and S.D. contributed new reagents/analytic tools; F.Z. and L.J. analyzed data; J.W. and C.L. provided funding; and F.Z., J.W., and C.L. wrote the paper.

The authors declare no competing interest.

This article is a PNAS Direct Submission.

[1]To whom correspondence may be addressed. Email: biomatwj@163.com or liucs@ecust.edu.cn.

This article contains supporting information online at https://www.pnas.org/lookup/suppl/doi:10.1073/pnas.2410579121/-/DCSupplemental.

Published November 20, 2024.

caused by inflammatory factors, we attempt to use osteo-organoids developed from biomaterials loaded with BMP-2 as the licensing sites for MSCs. Our previous research indicates that osteo-organoids not only produce MSCs and hematopoietic stem cells but also contain numbers immune cells capable of secreting various inflammatory factors (23). This implies that the newly formed bone-like tissue serves not only as a reservoir of MSCs but also as an artificial inflammatory microenvironment in vivo. The complexity of this environment may confer unexpected properties to the derived MSCs. While the influence of tissue inflammatory microenvironments on MSC immunomodulatory is recognized, the underlying mechanism remains unclear, with osteo-organoids offering valuable tools for further exploration. Furthermore, the role of scaffold materials in osteo-organoids has been overlooked previously, despite evidence that biomaterial components significantly impact the host's inflammatory response (24). Hence, understanding the impact of the composition of research materials on the inflammatory microenvironment of osteo-organoids is a critical issue for further investigation.

In this study, we found that the inflammatory state of the tissue microenvironment within osteo-organoids is modulated by material composition. Specifically, polysaccharide-based materials induce higher inflammation than protein-based materials, enhancing MSCs immunomodulatory abilities. MSCs derived from hyaluronic acid methacryloyl (HAMA)-based osteo-organoids (HMSCs) promote macrophage polarization from M1 to M2, inhibit T cell proliferation, and induce Treg differentiation via PGE2 secretion. Compared to bone marrow–derived MSCs (BMSCs) treated with IFN-γ, HMSCs exhibit lower immunogenicity, favoring their persistence within the host. Additionally, due to alterations in DNA methylation levels of PGE2 synthesis-related genes, HMSCs maintain their immunomodulatory abilities after multiple passages. Therapeutic efficacy was confirmed in a dextran sulfate sodium (DSS)-induced colitis model, reshaping the inflammatory ecosystem. These results suggest that constructing an in vivo inflammatory niche for MSCs through osteo-organoids is an effective strategy for licensing their immunomodulatory function.

Results

Controllable Inflammatory Microenvironment of Osteo-Organoids Licenses the Immunoregulatory Functions of MSCs. The scaffolds (Sca) loaded with BMP-2 can develop into osteo-organoids within the host body. Our prior investigation delineated this process into three stages: fibrous proliferation, osteochondral differentiation, and BM generation, with a notably higher proportion of immune cells during the fibrous proliferation phase compared to the BM phase (23). Naive MSCs require priming by cytokines from immune cells in the inflammatory environment (25, 26). Material composition can influence immune cell fate and tissue inflammation (27). Motivated by these findings, we hypothesize that early-stage osteo-organoids represent the optimal time point for MSC licensing and that the composition of biomaterials influences the inflammatory response during this phase. To investigate, we used protein-based materials [gelatin, gelatin methacryloyl (GelMA), and silk fibroin methacryloyl (SilMA)] and polysaccharide-based materials (HAMA, sodium alginate, chitosan), identifying synthesized HAMA through 1H NMR and FT-IR (*SI Appendix*, Fig. S1 *A* and *B*). We loaded 30 μg BMP-2 onto Sca, freeze-dried them, and implanted them subcutaneously in mice. BMP-2 initiated the osteogenic process in all groups (*SI Appendix*, Fig. S1*C*). Histological analysis showed BMP-2 induced the formation of a fibrous envelope around the material after 1 wk of implantation, with numerous chondrocytes (Cc) embedded within it. By the second and third weeks, the Cc differentiated into osteocytes and the bone tissue gradually matured (Fig. 1*A* and *SI Appendix*, Fig. S1*D*). Notably, the fibrous tissue (Ft) disappeared entirely after 2 wk of implantation in the protein-based material group, whereas the polysaccharide-based material group retained the fibrous layer structure between the newborn bone and the material (*SI Appendix*, Fig. S1*D*), indicating a stronger inflammatory response. Neutrophils and macrophages, by secreting various inflammatory and chemotactic factors, are the principal drivers of local tissue inflammation (28, 29). Consistent with the histological findings, flow cytometry analysis showed a higher proportion of neutrophils ($CD45^+CD11b^+Ly6G^+$ cells) and macrophages ($CD45^+CD11b^+F4/80^+$ cells) in polysaccharide-based osteo-organoids at each time point (Fig. 1 *B* and *C* and *SI Appendix*, Fig. S2 *A–C*). Meanwhile, the proportion of immune cells decreased over time, marking fibrous proliferation as the peak inflammatory stage. The changes in macrophage subtype proportions also supported this pattern: The polysaccharide group had more proinflammatory macrophages (M1). In each group, M1 macrophage proportions decreased while M2 macrophages increased over time (Fig. 1 *D* and *E* and *SI Appendix*, Fig. S2*D*). Notably, there was no significant difference in macrophage subtype proportions between groups in the third week (Fig. 1 *D* and *E*). These results suggest that polysaccharide materials can create a more pronounced inflammatory environment in osteo-organoids, potentially enhancing MSC immunomodulatory capabilities to alleviate internal inflammation. To further validate this conclusion, we used ELISA to measure the levels of inflammatory factors in the osteo-organoids at 1 wk, such as IL-1β, IFN-γ, and TNF-α, that can license MSCs. The results demonstrated that during the fibrous proliferation phase, the levels of inflammatory cytokines in the osteo-organoids were significantly higher than in the mouse femurs, with the polysaccharide group exhibiting elevated levels compared to the protein group (Fig. 1*F*).

To investigate why polysaccharide-based materials induce a stronger inflammatory microenvironment, we implanted fluorescently labeled hydrogels subcutaneously in mice. In vivo imaging revealed no leakage of the fluorescence signal after 1 wk, with stable signal intensity, indicating that the material did not degrade. This finding rules out the possibility that degradation products from the polysaccharide caused the inflammatory microenvironment (*SI Appendix*, Fig. S3 *A* and *B*). Meanwhile, numerous studies have indicated that high doses of BMP-2 can induce inflammation during bone generation (30). We observed no fibrous capsule formation occurred around the scaffold + PBS implants after 1 wk (*SI Appendix*, Fig. S3*C*), suggesting that BMP-2 is the primary factor for both osteo-organoid induction and inflammatory microenvironment creation. Subsequently, we analyzed BMP-2 release rates across groups, finding that polysaccharide-based materials exhibited a stronger sustained-release effect than protein-based materials (*SI Appendix*, Fig. S3*D*). Given BMP-2's short half-life in the physiological environment (31), rapid release may lead to insufficient activity during early osteo-organoid development, possibly explaining the weaker inflammatory microenvironment in protein-based models.

To explore the correlation between inflammatory levels in the osteo-organoid microenvironment and MSC immunomodulatory function, we conducted coculture experiments of MSCs and immune cells. MSCs were obtained from 1-wk-old osteo-organoids and purified through multiple passaging in vitro culture (32). Flow cytometry analysis showed over 95% expression of MSC surface markers CD44, CD29, CD105, and Sca-1, with no expression of CD45, CD34, CD11b, or CD31 (*SI Appendix*, Fig. S4). M1 macrophages were obtained by polarizing mouse BM–derived

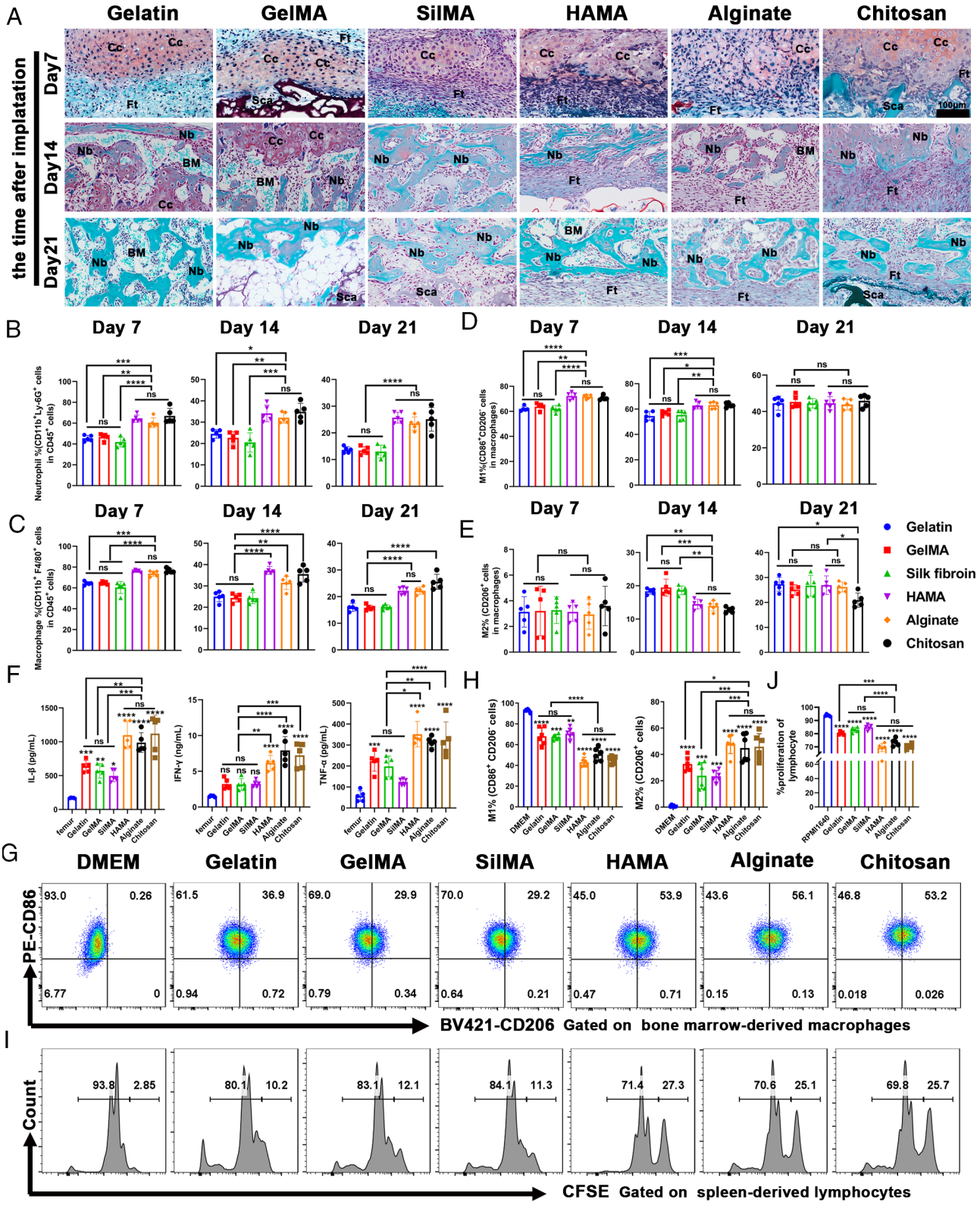

Fig. 1. Characterization of the inflammatory niche in osteo-organoids. (*A*) Saffron O/Fast green staining of osteo-organoids at weeks 1, 2, and 3 after implantation. (Scale bar, 100 μm.) Ft, Sca, Cc, BM, and new bone (Nb) are shown. (*B*–*E*) Flow cytometry quantitative analysis of neutrophils ($CD45^+CD11b^+Ly6G^+$cells), macrophages ($CD45^+CD11b^+F4/80^+$cells), M1 macrophages ($CD86^+CD206^-$ cells), and M2 macrophages ($CD206^+$ cells) in the osteo-organoids at weeks 1, 2, and 3 after implantation ($n = 5$). (*F*) The levels of TNF-α, IL-1β, and IFN-γ within the osteo-organoids were determined by ELISA ($n = 5$). (*G* and *H*) Representative flow cytometry plots (*G*) with quantification (*H*) of polarization of M1 macrophages ($CD86^+CD206^-$ cells) toward M2 ($CD206^+$ cells) on day 5 after treatment with MSCs ($n = 6$). (*I* and *J*) Representative flow cytometry plots (*I*) and quantification (*J*) of $CFSE^+$ T cells on day 3 after coculture with MSCs ($n = 5$). Data are presented as means ± SD. The Shapiro–Wilk test was employed to assess the normal distribution of the data. Statistical differences among groups were identified by one-way ANOVA, followed by Tukey's multiple comparison tests. $^*P < 0.05$, $^{**}P < 0.01$, $^{***}P < 0.005$, and $^{****}P < 0.0001$; ns denotes no significant difference.

macrophages with 100 ng/mL LPS and 30 ng/mL IFN-γ for 48 h (33, 34); lymphocytes were extracted from the spleens of mice. Our results indicate that MSCs from the polysaccharide-based material group had higher anti-inflammatory capabilities and greater inhibition of activated lymphocyte proliferation compared to the protein-based group (Fig. 1 *G–J*). This suggests a positive correlation between osteo-organoids inflammatory level and MSC immunomodulatory capacity. These findings highlight the feasibility of utilizing BMP-2-induced osteogenic development to generate substantial MSCs quantities and an inflammatory niche, thereby activating MSC immunomodulatory function in vivo.

Leptin Receptor (LepR) and Pdgfrα (CD140α) are markers highly enriched in BMSCs (35, 36). We assessed the proportion of MSCs ($CD45^-Ter119^-CD31^-CD11b^-PDGFR\alpha^+$ cells) in osteo-organoids at various time points using flow cytometry. Specifically, the proportion of MSCs in the 1-wk-old osteo-organoid group increased by 4.17~15.17-folds compared to native BM, subsequently decreasing to the level of native BM in later developmental stages (*SI Appendix*, Fig. S5 *A* and *B*). This trend was consistent across all materials used, indicating the broad applicability of the osteo-organoid construction method. Hyaluronic acid, a CD44 ligand on MSCs, could significantly recruit MSCs (37), which may explain slower decline in MSC proportion observed in the HAMA group during late stage of osteogenesis (*SI Appendix*, Fig. S5 *A* and *B*).

Trilineage differentiation experiments revealed heterogeneity among MSCs derived from osteo-organoids constructed with different materials. Specifically, MSCs in the sodium alginate group favored chondrogenic differentiation, while those in the chitosan group showed a preference for osteogenic differentiation. MSCs in the SilMA group exhibited weaker differentiation overall. In contrast, MSCs in the GelMA and HAMA groups demonstrated a more balanced differentiation capability into bone, cartilage, and adipose tissues, exhibiting enhanced stemness and differentiation potential (*SI Appendix*, Fig. S6 *A* and *B*). Previous literature has reported that the stiffness of the tissue microenvironment can influence the differentiation fate of MSCs (38, 39). We therefore tested the stiffness of the hydrogel Sca. The results showed that the storage modulus of each hydrogel was below 1,000 Pa, which does not meet the conditions required for stiffness to influence MSC differentiation (*SI Appendix*, Fig. S6*C*). Chitosan serves as a potential osteogenic factor with effects comparable to dexamethasone (40), while calcium ions promote chondrogenic differentiation of mesenchymal cells in a dose-dependent manner (41). These biological effects of these materials may explain the pronounced differentiation tendencies in MSCs derived from chitosan and sodium alginate groups, whereas the rapid inactivation of BMP-2 likely contributes to the inferior differentiation capability of SilMA-based MSCs. Considering the immunomodulatory function and multidirectional differentiation ability of MSCs, we selected hyaluronic acid as the scaffold material for constructing osteo-organoids, referring to MSCs derived from HAMA osteo-organoids as HMSCs.

HMSCs Exert Immunoregulatory Effects through the Secretion of PGE2. To further investigate the changes in immunomodulatory function of HMSCs throughout the development of HAMA-based osteo-organoids, we conducted histological analyses. Immunofluorescence staining revealed that LepR-positive MSCs were predominantly located in the fibrous layer during the first week, which provided an inflammatory niche for HMSCs. By the second week, HMSCs migrated to the newly formed bone outside the fibrous layer, coinciding with reduction inflammation in the surrounding area (Fig. 2*A*). Immunohistochemistry revealed significant decreases in CD11b, IL-1β, and myeloperoxidase (MPO) levels during development, displaying similar spatiotemporal patterns to HMSCs (Fig. 2 *A* and *B*). Additionally, the fibrous layer thickness of HAMA-based osteo-organoids gradually diminished (*SI Appendix*, Fig. S7*A*), and the levels of inflammatory factors decreased correspondingly (*SI Appendix*, Fig. S7*B*). Moreover, the proportion of neutrophils and macrophages in the organoids gradually reverted to normal levels after peaking in the first week (*SI Appendix*, Fig. S7 *C* and *D*). These data conclusively demonstrated that the inflammatory level of the HMSC niche was highest during the initial week of osteo-organoid development.

To evaluate the immunomodulatory function of HMSCs at three developmental stages, we cocultured them with M1 macrophages. HMSCs obtained at week 1 (1W-HMSCs) induced a higher proportion of M2 macrophages, with efficacy decreasing over time (*SI Appendix*, Fig. S7 *E* and *F*). This decline in anti-inflammatory capacity correlated with the decreasing inflammation levels in HAMA-based osteo-organoids, consistent with previous observations. In the colony-forming unit-fibroblast (CFU-F) experiment, the 1W-HMSC group demonstrated superior self-renewal capability. In contrast, 2W-HMSCs and 3W-HMSCs showed no significant difference in colony formation compared to BM–derived MSCs (*SI Appendix*, Fig. S7 *G* and *H*). Overall, the first week postimplantation was identified as the optimal timeframe for activating the immunomodulatory capabilities of HMSCs.

To further investigate the similarities and distinctions between in vivo activation by the inflammatory microenvironment and in vitro treatment with inflammatory factors on MSCs, we evaluated the immunomodulatory function of BMSCs treated with 20 ng/mL IFN-γ for 48 h (IBMSCs), with untreated BMSCs serving as the control. qPCR detected immune regulatory-related genes across the three MSC types. Results showed upregulation of Ptgs2, Inos, and Ido, alongside downregulation of Tgf-β and Tsg-6 in both IBMSCs and HMSCs compared to BMSCs. Ptgs2 and Inos encode key synthases for PGE2 and NO, critical immunomodulatory factors secreted by mouse MSCs (4, 42, 43). Notably, Ptgs2 was the most significantly upregulated gene in HMSCs, increasing 113.4-fold and 20.25-fold compared to BMSCs and IBMSCs, respectively (Fig. 2*C*), suggesting Ptgs2 may be a primary pathway for HMSCs' immunoregulatory effects. Further analysis revealed significantly higher COX-2 (PTGS2) protein levels in HMSCs compared to BMSCs and IBMSCs. ELISA confirmed that PGE2 concentrations in HMSC culture supernatants were significantly higher, measuring 8.27 times that of BMSCs and 3.09 times that of IBMSCs (Fig. 2*F*). The concentration of NO in HMSC culture medium was significantly higher than in BMSCs but slightly lower than in IBMSCs (Fig. 2*G*), indicating that the two activation methods may exert different effects on MSCs. To further assess PGE2's role in HMSCs' immunomodulatory effects, we treated HMSCs with Celecoxib, a selective COX-2 inhibitor. This treatment significantly suppressed COX-2 expression and PGE2 secretion in HMSCs (Fig. 2 *H–J*).

Flow cytometry and immunofluorescence staining showed HMSCs induced a greater polarization of macrophages from M1 to M2 compared to IBMSCs and BMSCs. Additionally, celecoxib abolished the anti-inflammatory function of HMSCs (Fig. 2 *K* and *L* and *SI Appendix*, Fig. S8*A*). We assessed the gene expression profile of macrophages cocultured with MSCs. qPCR analysis revealed that HMSCs downregulated M1-related genes TNF-α and CD86 more effectively, while upregulating M2-related genes Arg-1 and CD206 compared to the other MSC groups (*SI Appendix*, Fig. S8*B*). Among anti-inflammatory M2 phenotypes, subsets such as M2a, M2b, and M2c are recognized (44).

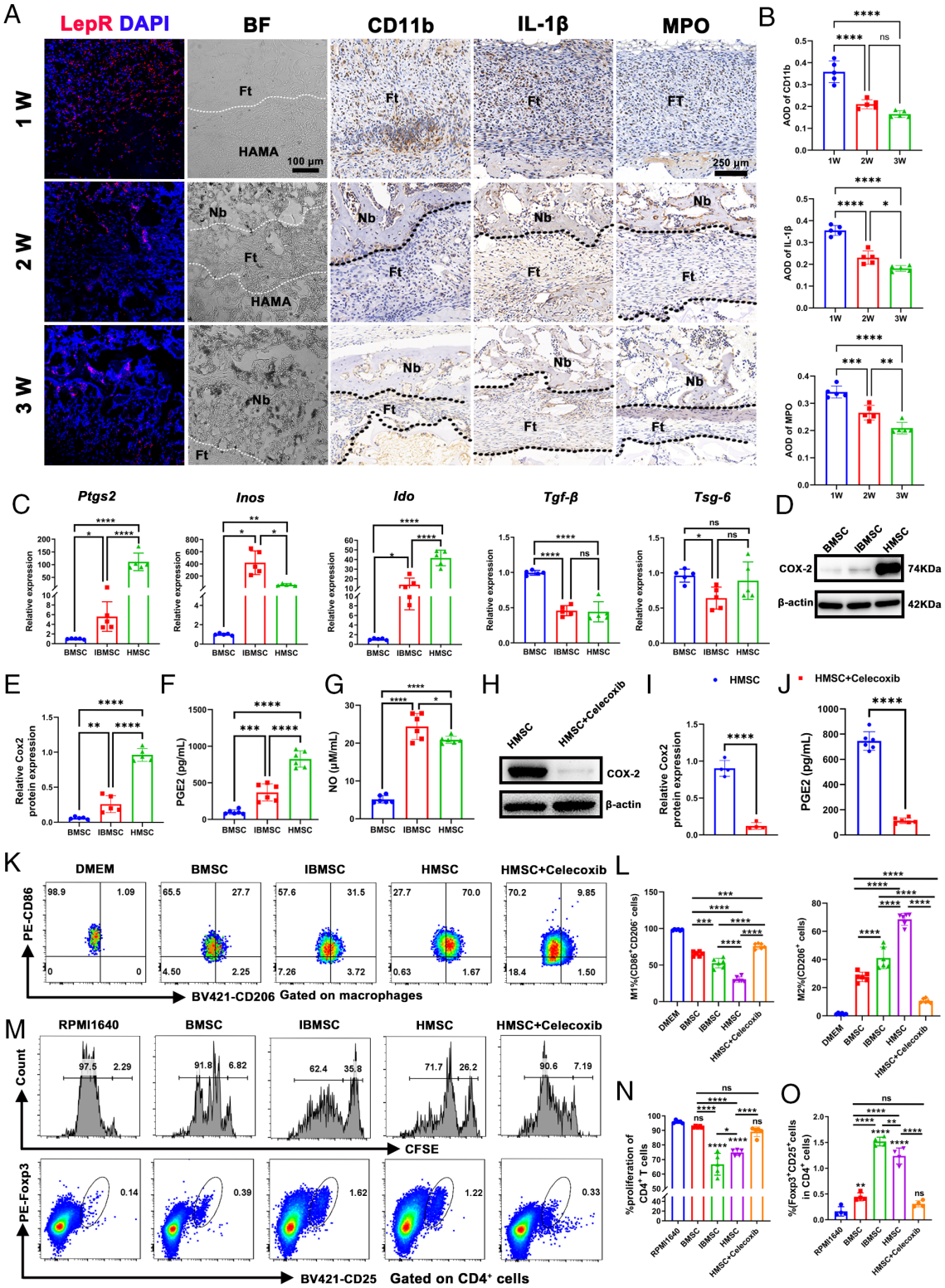

Fig. 2. Characterization of the immunomodulatory function of HMSCs. (*A*) Representative immunostainings of Lepr$^+$ MSCs and immunohistochemical staining of CD11b, IL-1β, and MPO in HAMA-based osteo-organoids at weeks 1, 2, and 3 after implantation. Lepr$^+$ MSCs are shown in red and DAPI is shown in blue (nucleus). Ft, Nb. (Scale bar, 100 μm and 250 μm.) (*B*) Quantification analysis of CD11b, IL-1β, and MPO positive area (n = 5). Average optical density (AOD). (*C*) Relative immunomodulation-related mRNA expressions of MSCs (n = 5). (*D* and *E*) Western blot analysis (*D*) and the quantitation analysis of relative levels (*E*) of cellular COX-2 (n = 5). (*F*) ELISA of the concentration of PGE2 in the culture supernatant of MSCs (n = 6). (*G*) Detection of NO levels in the culture supernatant of MSCs (n = 6). (*H* and *I*) Western blot analysis (*H*) and the quantitation analysis of relative levels (*I*) of cellular COX-2 in HMSC treated with celecoxib (n = 4). (*J*) ELISA of the concentration of PGE2 in the culture supernatant of HMSC treated with celecoxib (n = 6). (*K* and *L*) Representative flow cytometry plots (*K*) and quantification analysis (*L*) of polarization of M1 macrophages toward M2 on day 5 after treatment with MSCs. (n = 6). (*M*–*O*) Representative flow cytometry plots (*M*) and quantification of CFSE$^+$ T cells (*N*) (n = 5) and Tregs(O) (CD4$^+$CD25$^+$FoxP3$^+$ cells) on day 3 after coculture with MSCs (n = 4). Data are presented as means ± SD. The Shapiro–Wilk test was employed to assess the normal distribution of the data. Statistical differences among groups were identified by t tests (*I* and *J*) or one-way ANOVA, followed by Tukey's multiple comparison tests. *P < 0.05, **P < 0.01, ***P < 0.005, and ****P < 0.0001; ns denotes no significant difference.

MSCs treated with IFN-γ are known to promote M2b polarization, which is thought to regulate immunity while minimizing tissue damage (45, 46). Encouragingly, HMSCs similarly facilitated macrophage polarization toward M2b and M2c phenotypes (*SI Appendix*, Fig. S8*C*). Parallelly, coculturing mouse spleen–derived T cells with these MSCs revealed that both HMSC and IBMSC groups inhibited T cell proliferation and promoted regulatory T cell (Treg) differentiation. However, celecoxib treatment compromised the immunomodulatory function of HMSCs (Fig. 2 *M*–*O*). In summary, these findings strongly indicate that during the fibrous proliferation phase, the immunomodulatory function of HMSCs is activated by the unique inflammatory microenvironment of in vivo osteo-organoids, operating through the secretion of high levels of PGE2.

An important question to consider is whether in vivo incubation in osteo-organoids is necessary for HMSCs to exhibit their immunomodulatory functions. To simulate the conditions that license HMSCs, we treated BMSCs in vitro with BMP-2, IFN-γ, and IL-1β. qPCR results showed that the gene expression profile of multifactor-treated BMSCs did not resemble that of HMSCs (*SI Appendix*, Fig. S9*A*), and the secretion level of PGE2 was significantly lower than in HMSCs (*SI Appendix*, Fig. S9*B*). BMP-2 effectively induces osteogenic differentiation of BMSCs in vitro (47). Consequently, we evaluated osteogenic-related gene expression in both cell types, finding that multi-factor-treated BMSCs exhibited a greater tendency for osteogenic differentiation (*SI Appendix*, Fig. S9*C*). This suggests that multifactor treatment leads to the loss of stemness in BMSCs. Coculture experiments revealed that multi-factor-treated BMSCs had significantly lower anti-inflammatory capacity and inhibited T cell proliferation compared to HMSCs (*SI Appendix*, Fig. S9 *D*–*G*). The above results indicate that treating BMSCs with BMP-2, IFN-γ, and IL-1β could not achieve the same immunomodulatory effects as HMSCs. Thus, the licensing effect of osteo-organoids on HMSCs appears to involve complex physiological interactions between inflammation and development.

Comparative Analysis of Gene Expression Profiles between HMSCs and IBMSCs. To elucidate the impact of the inflammatory microenvironment in osteo-organoids on HMSCs, we conducted bioinformatics analysis on BMSCs, IBMSCs, and HMSCs at passage 2, using BMSCs as controls. Principal component analysis (PCA) revealed distinct transcriptomic clustering among the groups (*SI Appendix*, Fig. S10*A*). The common differentially expressed genes (CDEGs) were identified by intersecting the DEGs between IBMSCs vs. BMSCs, and HMSCs vs. BMSCs (*SI Appendix*, Fig. S10*B*). Cluster analysis showed that the top 100 significant CDEGs indicated expression patterns in HMSCs similar to IBMSCs (*SI Appendix*, Fig. S10*C*).

Biological process enrichment analysis revealed that the DEGs in IBMSCs vs. BMSCs were enriched in immune response and inflammatory response pathways, consistent with the effects of inflammatory factor treatment (*SI Appendix*, Fig. S10*D*). Notably, the enrichment pathways of DEGs in HMSCs vs. BMSCs mirrored those of IBMSCs (*SI Appendix*, Fig. S10 *E* and *F*). Furthermore, Gene-set enrichment analysis (GSEA) indicated downregulation of immune and inflammatory response signature genes in HMSCs, whereas these genes were upregulated in IBMSCs (*SI Appendix*, Fig. S10 *G* and *H*). This discrepancy may stem from differing MSC responses to licensing: IFN-γ treatment induced an inflammatory state in IBMSCs, reflected by upregulation of pathways such as TNF and NF-kappa B (*SI Appendix*, Fig. S10*I*). Conversely, HMSCs in the inflammatory microenvironment displayed a noninflammatory state (*SI Appendix*, Fig. S10*J*). We categorized DEGs into upregulated and downregulated subsets, identifying overlapping genes for further analysis (*SI Appendix*, Fig. S10*B*). Cluster and biological process enrichment analysis of upregulated CDEGs identified *Ptgs2* gene and positive regulation prostaglandin biosynthetic process in IBMSCs and HMSCs (*SI Appendix*, Fig. S11 *A* and *B*). This underscores the activation of immune regulatory genes in HMSCs in response to the inflammatory microenvironment of osteo-organoids. Overall, the inflammatory context effectively triggers the immunomodulatory function of MSCs, differing from direct exposure to inflammatory factors, leading to a gentler impact and distinct characteristics.

HMSCs Exhibit Decreased Immunogenicity and Heightened Resistance to Inflammatory Stimuli and Oxidative Stress. The Kyoto Encyclopedia of Genes and Genomes (KEGG) pathway enrichment analysis showed that CDEGs in IBMSCs and HMSCs were enriched in the antigen processing and presentation pathway (Fig. 3*A*). Consistent with previous literature, GSEA revealed enhanced antigen processing and presentation signaling in IFN-γ-treated BMSCs, whereas the signaling was significantly downregulated in HMSCs (Fig. 3*B*). Cluster analysis revealed that genes related to antigen processing and presentation, such as *H2-DMa*, *H2-DMb1*, and *Tap1*, were least expressed in HMSCs (*SI Appendix*, Fig. S12), suggesting that HMSCs may possess enhanced immune privilege. Research indicates that IFN-γ induces MHC-II expression in mouse BMSCs, enhancing antigen presentation and reducing immunogenicity, mediated by the type IV CIITA promoter regulated by Stat1 and IFN regulatory factor 1 (IRF-1) (20, 48, 49). To assess immunogenicity, BMSCs and HMSCs were treated with IFN-γ, followed by flow cytometry for MHC-II expression. Results showed significantly lower MHC-II levels in HMSCs compared to BMSCs (Fig. 3 *C* and *D*). Additionally, qPCR analysis revealed significant upregulation of Ciita expression in BMSCs post-IFN-γ treatment, while HMSCs showed no significant change (Fig. 3*E*). This indicates that HMSCs are less sensitive to exogenous inflammatory stimuli, enhancing their clinical potential. To explore the underlying mechanism, we analyzed MHC-II expression pathways through western blot experiments. Results indicated that while Stat1 phosphorylation was normal in HMSCs, IRF-1 expression was notably lower compared to BMSCs (Fig. 3 *F*–*I*), suggesting that reduced IRF-1 in HMSCs hinders MHC-II induction by IFN-γ. Furthermore, to ascertain whether HMSCs exhibit resistance to other stressors, we stimulated MSCs with LPS and H_2O_2, respectively. Flow cytometry revealed a lower apoptosis rate in HMSCs compared to BMSCs, with no significant difference from controls (Fig. 3 *J*–*L*). Collectively, these findings suggest that HMSCs derived from osteo-organoids possess reduced immunogenicity and increased resistance to inflammatory stimuli and oxidative stress, enhancing their survival potential in disease microenvironments.

In Vivo Licensing of HMSC Immunomodulatory Function Is Sustained after Prolonged Cultivation. While inflammatory factors can enhance the immunomodulatory capacity of MSCs, this effect is typically transient. Previous studies have indicated that genes upregulated in BMSCs following IFN-γ or IL-1β treatment exhibit significant downregulation after prolonged culture periods (50). This raised the question of whether the immunomodulatory function of HMSCs, activated by the inflammatory microenvironment, also exhibits transience. We conducted a long-term monitoring experiment on IBMSCs and HMSCs starting from the second passage. IBMSCs cultured for 7 days (7D-IBMSC) showed a marked decrease in immunomodulatory function, evidenced by reduced macrophage polarization from M1 to M2 phenotypes (Fig. 4 *A* and *B* and *SI Appendix*, Fig. S13 *A* and *B*). In contrast, HMSCs

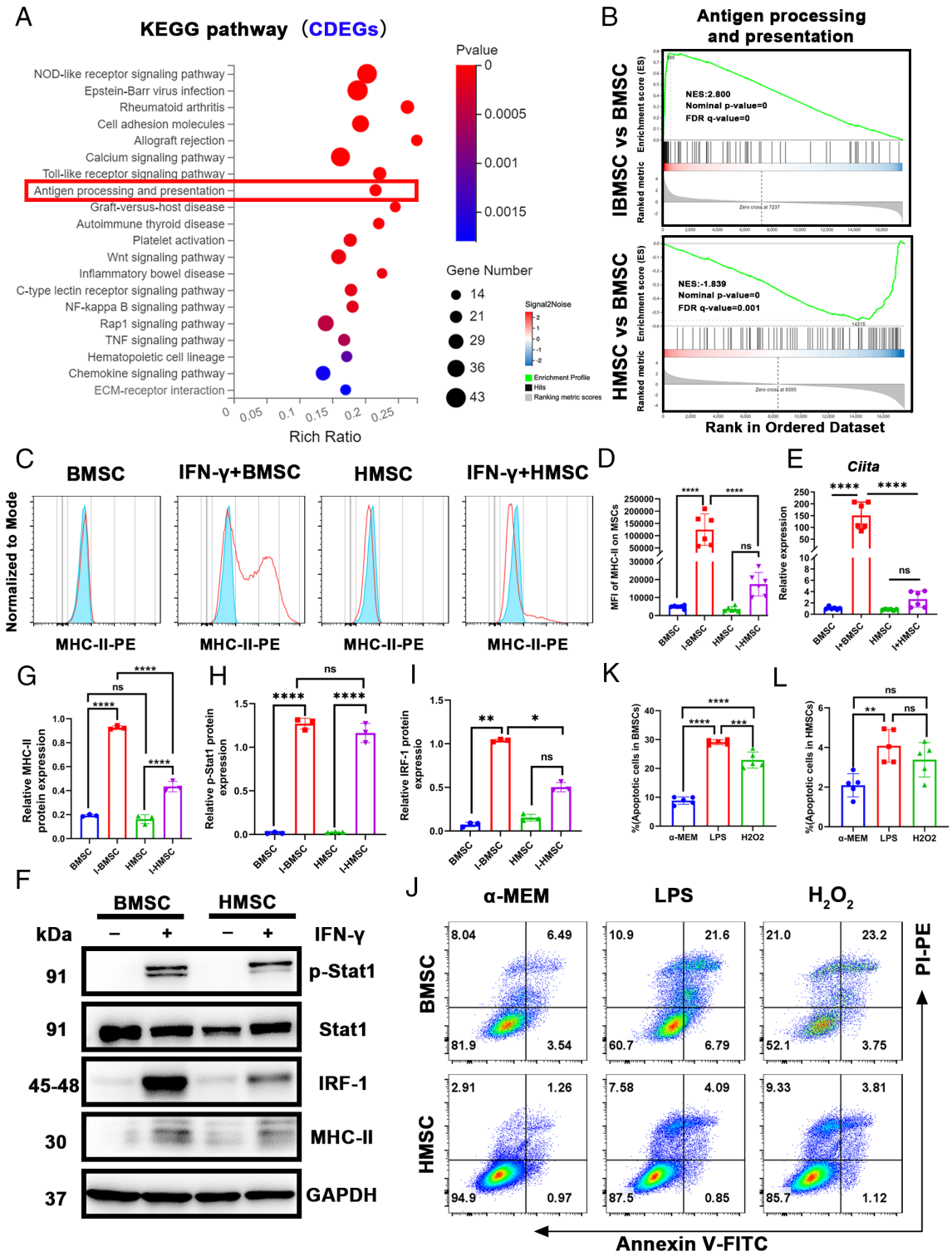

Fig. 3. HMSCs exhibit lower immunogenicity. (*A*) Representative KEGG pathways of common significantly DEGs (CDEGs). ($P \leq 0.05$, |log fold change| ≥ 1). (*B*) GSEA plots of MSCs from IBMSC vs. BMSC and HMSC vs. BMSC (|NES| > 1, Nominal *P*-value < 0.05, FDR < 0.25). (*C*) Representative flow cytometry histograms of the median fluorescence intensity (MFI) of MHC-II on MSCs. (*D*) Analysis of the MFI of MHC-II on MSCs ($n = 6$). (*E*) qPCR analysis of *Ciita* mRNA expression in MSCs ($n = 6$). (*F–I*) Western blot analysis (*F*) and the quantitation of relative level (*G–I*) of phosphorylated Stat1, total Stat1, IRF-1, and MHC-II in MSCs ($n = 3$). (*J–L*) Representative flow cytometry plots (*J*) and quantification (*K* and *L*) of apoptosis of MSCs after 3 d treatment with LPS and H_2O_2 ($n = 5$). Data are presented as means ± SD. The Shapiro–Wilk test was employed to assess the normal distribution of the data. Statistical differences among groups were identified by one-way ANOVA, followed by Tukey's multiple comparison tests (*D*, *E*, *K*, and *L*). When n = 3, statistical differences among groups were assessed using the Kruskal–Wallis test (*G–I*). $^{*}P < 0.05$, $^{**}P < 0.01$, $^{***}P < 0.005$, and $^{****}P < 0.0001$; ns denotes no significant difference.

exhibited a consistent ability to induce more M2 macrophages after three passages (Fig. 4 *A* and *B* and *SI Appendix*, Fig. S13 *A* and *B*). The sustained immunomodulatory effects of HMSCs suggest an epigenetic memory, with DNA methylation playing a key role in stabilizing gene expression patterns and maintaining specific phenotypic traits during cell division. Methylation marks can be inherited across generations, preserving memory related to developmental stages or environmental adaptations (51). To verify this, we compared the DNA methylation profiles of BMSCs, IBMSCs, and HMSCs using reduced representation bisulfite

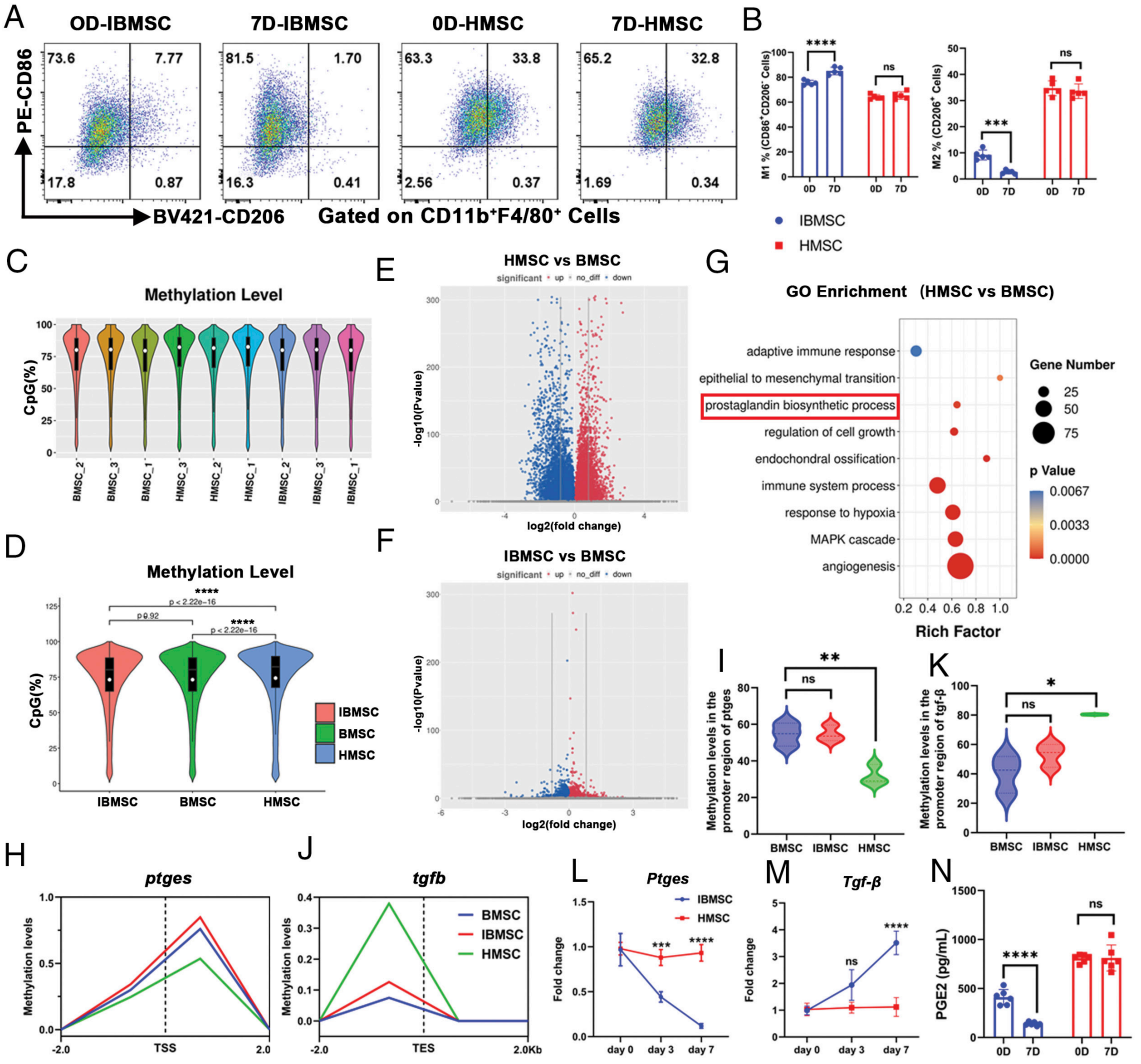

Fig. 4. The immunomodulation function of HMSC is long-lasting. (*A* and *B*) Representative flow cytometry plots (*A*) and quantification (*B*) of M1 macrophages ($CD86^+CD206^-$ cells) and M2 macrophages ($CD206^+$ cells) on day 7 after coculture with MSCs ($n = 5$). (*C*) DNA methylation rate under the contexts of CpG in BMSCs, IBMSCs, and HMSCs by RRBS. (*D*) Quantification analysis of DNA methylation rates in CpG regions. (*E* and *F*) Analysis of DMRs using a volcano plot. DMR analysis was conducted using the R package methyl Kit, with default settings of 1,000 bp windows and 500 bp overlap. An FDR (adjusted *P*-value) < 0.05 was used as the threshold for differential selection. Red indicates upregulated DMRs, while blue indicates downregulated DMRs. (*G*) GO enrichment analysis for DMGs in HMSC vs. BMSC. The color of the dot indicates the *P*-value and the size of the dot represents the enrichment score. (*H* and *I*) Visualization and quantitative statistics of DNA methylation levels in the promoter region of Ptges. TSS: The starting positions of the corresponding transcript. (*J* and *K*) Visualization and quantitative statistics of DNA methylation levels in the promoter region of Tgf-β. TES: The ending positions of the corresponding transcript. (*L* and *M*) q-PCR analysis of Ptges and Tgf-β in MSCs cultured in vitro for 7 d ($n = 5$). (*N*) ELISA of the concentration of PGE2 in the culture supernatant of MSCs ($n = 6$). Data are presented as means ± SD. The Shapiro–Wilk test was employed to assess the normal distribution of the data. Statistical differences among groups were identified by two-way ANOVA, followed by Tukey's multiple comparison tests Data (*B* and *L*–*N*). When n = 3, statistical differences among groups were assessed using the Kruskal–Wallis test (*I* and *K*). *$P < 0.05$, **$P < 0.01$, ***$P < 0.005$, and ****$P < 0.0001$; ns denotes no significant difference.

sequencing (RRBS). Principal component analysis (PCA) revealed no distinct clustering for BMSCs and IBMSCs, while HMSCs showed clear separation from both groups (*SI Appendix*, Fig. S14*A*), indicating a unique DNA methylation profile. Violin plots indicated significantly higher DNA methylation levels in both the whole genome and CpG regions of HMSCs compared to BMSCs and IBMSCs, with no significant difference between IBMSCs and BMSCs (Fig. 4 *C* and *D* and *SI Appendix*, Fig. S14 *B* and *C*). This suggests that IFN-γ treatment does not significantly affect the DNA methylation levels of BMSCs.

Next, we calculated differentially methylated regions (DMRs) among BMSCs, IBMSCs, and HMSCs to explore the relationship between methylation differences and the immunoregulatory functions of stem cells. Clearly, the number of DMRs in the promoter areas of HMSC was significantly higher than that in IBMSC, with promoters serving as switches for gene expression (*SI Appendix*, Fig. S14 *D* and *E*). The volcano plot confirmed significant differences in DNA methylation levels between HMSCs and BMSCs, while IBMSCs displayed smaller differences clustered in the lower middle region (Fig. 4 *E* and *F*). GO enrichment analysis of differentially methylated region-related genes (DMGs) in HMSCs vs. BMSCs revealed significant enrichment in immunomodulatory functions, including adaptive immune response, prostaglandin biosynthetic process, and response to hypoxia (Fig. 4*G*).

Generally, DNA methylation inhibits gene expression by preventing transcription factor binding in promoter and regulatory regions (52). Therefore, we further analyzed the methylation levels of Ptges and Mif, which are associated with PGE2 synthesis in the prostaglandin biosynthetic pathway (53). Compared to BMSCs, HMSCs exhibited hypomethylation in the promoter regions of Ptges and Mif, indicating active PGE2 synthesis (Fig. 4 *H* and *I* and *SI Appendix*, Fig. S14*F*). Conversely, genes that inhibit PGE2 synthesis, such as Tgf-β and Pparg, showed hypermethylation in HMSCs (Fig. 4 *J* and *K* and *SI Appendix*, Fig. S14*G*) (54, 55). qPCR

validation revealed that while *Ptges* expression in IBMSCs significantly decreased after 7 d without IFN-γ treatment, HMSCs maintained levels similar to their initial state (Fig. 4*L*). Meanwhile, Tgf-β expression in IBMSCs gradually restored, with no significant changes in HMSCs (Fig. 4*M*). IBMSCs also showed reduced paracrine activity, leading to a significant decrease in PGE2 concentration in the culture supernatant, while HMSCs displayed the opposite trend (Fig. 4*N*). These findings suggest that during the development of bone organoids, the DNA methylation patterns in the genome of HMSC undergo changes involving various dynamic processes of de novo methylation and demethylation. These changes lead to the formation of a stable and unique DNA methylation pattern that exhibits immunomodulatory effects with epigenetic memory.

Transplanting HMSCs In Vivo Demonstrates Potent Protection against Colitis. In vivo effects of BMSCs, IBMSCs, and HMSCs were evaluated in a murine model of DSS-induced colitis (Fig. 5*A*). Following DSS treatment, the PBS-injected group exhibited a steady decline in body weight, with approximately 30% reduction by day 7. The treatment with HMSCs or IBMSCs significantly mitigated weight loss, while BMSCs had minimal impact (Fig. 5*B*). The survival rate of PBS-treated mice was merely 10% but increased to 20%, 60%, and 70% in BMSC, IBMSC, and HMSC-injected group, respectively (Fig. 5*C*). The disease activity index (DAI) evaluation on day 8 showed that both HMSC and IBMSC treatments effectively alleviated colitis severity, with HMSC treatment yielding the most favorable outcomes, while BMSCs exhibited little efficacy (Fig. 5*D*). Colon length, an intuitive indicator of colitis severity (56), was significantly preserved by MSC treatments, particularly by HMSCs (Fig. 5 *E* and *F*). Histological examination through H&E staining revealed severe epithelial ulceration, loss of goblet cells, and lymphocyte infiltration in PBS and BMSC-treated groups (Fig. 5*G*). In contrary, IBMSC and HMSC treatments significantly reduced DSS-induced colon damage, as reflected in histological scores (Fig. 5 *G* and *H*). Cytokine analysis of colon tissue indicated a significant reduction in proinflammatory cytokines IFN-γ, IL-1β, and TNF-α in MSC-treated groups, especially in the HMSC group, alongside increased levels of the anti-inflammatory cytokine IL-10 (Fig. 5*I*).

To elucidate the mechanisms underlying the therapeutic effects of HMSCs in colitis, we assessed the colonic ecosystem in mice on day 8. Immunohistochemistry revealed a significant reduction in immune cell infiltration, including T cells, macrophages, and neutrophils, in the colons of DSS-challenged mice treated with MSCs, with the HMSC group exhibiting superior efficacy (*SI Appendix*, Fig. S15 *A–D*). We then investigated the frequency and activation status of macrophages using immunofluorescence staining and flow cytometry. Consistently, both IBMSC and HMSC treatments led to a notable decrease in the proportion of macrophages in the colons of colitis mice compared to the BMSC-treated group. Additionally, HMSCs significantly promoted the polarization of macrophages toward the anti-inflammatory M2 phenotype (Fig. 5 *J–M* and *SI Appendix*, Fig. S15 *E–H*). The proportion of total macrophages and M2 subtypes in the colons of mice treated with HMSCs closely resembled those of the control group (Fig. 5 *J* and *M*). Furthermore, HMSC treatment led to a marked increase in CD4+CD25+Foxp3+ Tregs in the colonic tissue compared to the PBS-treated group (Fig. 5 *N* and *O*). Collectively, these findings suggest that the therapeutic efficacy of HMSCs arises from their ability to reshape the inflammatory ecosystem within the colons of colitis-afflicted mice.

Transplanted HMSCs Exhibit Prolonged Persistence in Host Mice. In vitro experiments revealed that HMSCs exhibited lower immunogenicity and stronger resistance to inflammatory stimuli and oxidative stress (Fig. 4). This prompted us to investigate whether HMSCs offer better engraftment capacity in vivo. To evaluate the persistence of transplanted MSCs, we tracked and quantified eGFP-labeled BMSCs, IBMSCs, and HMSCs injected intraperitoneally on days 0, 1, 3, 5, and 7 using a fluorescence-based in vivo cell tracking technique. Following administration, fluorescence imaging results indicated the presence of MSCs near the injection site (Fig. 6*A*). However, by day 3, the fluorescence intensity in the IBMSC group exhibited a significant decrease compared to the other two groups. By day 7, the IBMSC fluorescence signal had nearly vanished, while the HMSC signal maintained substantial intensity (Fig. 6 *A* and *B*). Subsequent immunofluorescence analysis confirmed the presence of both BMSCs and HMSCs, with notably higher abundance of HMSCs (Fig. 6 *C* and *D*). These findings indicate that HMSCs possess enhanced survival capabilities, indicating their greater potential for clinical application in challenging pathological microenvironments.

Discussion

The immunomodulatory capacity of MSCs is plastic and can be influenced by various biological, biochemical, and biophysical factors both in vivo and in vitro, through intricate interactions among cells, extracellular matrix, and soluble bioactive factors (57). Extensive evidence indicates that the therapeutic efficacy of MSC infusion significantly diminishes during periods of low inflammation at disease onset or recurrence (1), highlighting the pivotal role of tissue microenvironmental inflammation in modulating MSC immunomodulation function. The heterogeneous responsiveness to MSC therapy likely stems from variability in inflammatory conditions. Thus, leveraging the osteo-organoid platform to create a stable and controllable tissue microenvironment in vivo offers a promising strategy to precisely emulate settings conducive to licensing MSC immunomodulatory function.

Biomaterials, characterized by high controllability and unique biological effects, profoundly influence the physiological activities of cells, tissues, and organs (58). In the development of osteo-organoids, biomaterials serve as physical carriers for sustained protein release and provide a developmental locale while collaborating with BMP-2 to modulate the inflammatory cytokine profile of the tissue microenvironment, enhancing MSC effects. BMP-2-induced osteogenic development results in an augmented inflammatory microenvironment that is crucial for activating MSC immunomodulatory function. Moreover, osteo-organoids constructed with diverse biomaterials yield tissue-resident MSCs with distinct characteristics and differentiation propensities, catering to specific clinical needs such as bone repair, cartilage repair, and tendon healing. In addition, these MSCs demonstrate variations in immunomodulatory effects influenced by inflammatory niches, suggesting the potential to customize clinical treatments for specific inflammatory conditions, thus optimizing MSC-based protocols for precise fit of inflammatory responses at various disease stages.

Upon further characterization of HMSCs, we found a significant enrichment of genes related to immune and inflammatory responses, akin to IBMSCs (*SI Appendix*, Fig. S10 *D* and *E*), underscoring the influence of the inflammatory microenvironment of the osteo-organoids on HMSCs. Moreover, *Ptgs2*, as a key immunomodulation-related gene, was markedly upregulated in HMSCs, leading to increased levels of PGE2, which play a crucial role in inhibiting immune cell hyperactivity and reducing inflammation (59, 60). RNA-sequencing results revealed inhibited mTOR signaling in HMSCs (*SI Appendix*, Fig. S10*J*), which has been reported to improve the immunomodulatory properties of MSCs by enhancing the expression of COX-2 (61). This may elucidate the higher secretion of PGE2 by HMSCs. Notably, the

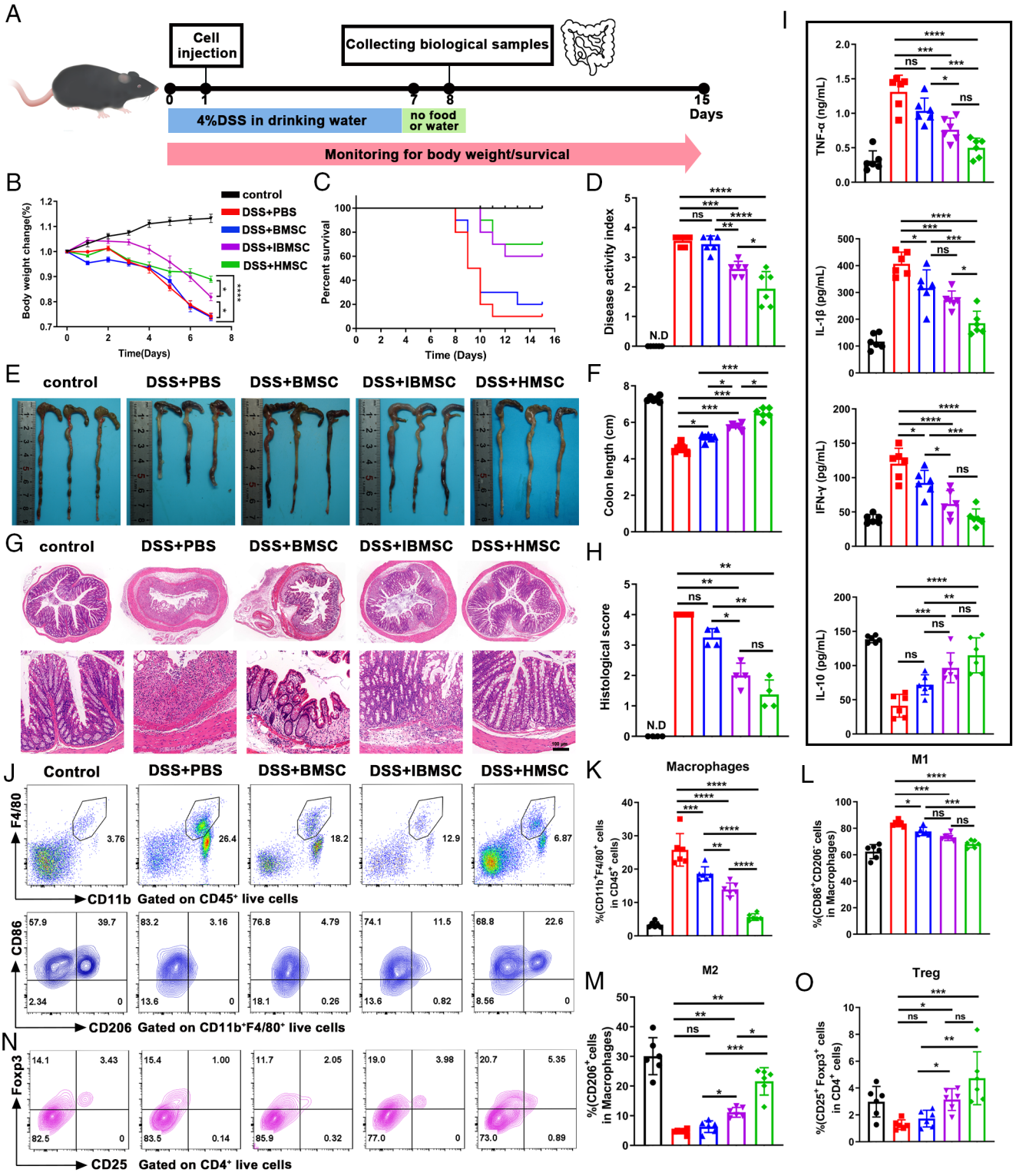

Fig. 5. Intraperitoneal injection of HMSCs ameliorates DSS-induced colitis. (*A*) Schematic representation of DSS-induced mouse colitis and MSCs treatment. (*B*) Body weight changes in colitis mice ($n = 6$). (*C*) Monitoring results for the survival rate presented as a percentage of day 0 value which was considered as 100% ($n = 10$). (*D*) DAI was calculated on day 7 ($n = 6$). No score for control was detected (N.D). (*E* and *F*) Macroscopic appearance (*E*) and the length of colons (*F*) from each group of mice were measured ($n = 6$). (*G*) Paraffin-embedded colon sections were stained with H&E for light microscopy assessment. (Scale bar, 100 μm.) (*H*) Histopathological score was assessed for disease severity ($n = 4$). (*I*) The levels of TNF-α, IL-1β, IFN-γ, and IL-10 within the colon tissue were determined by ELISA ($n = 6$). (*J*–*O*) Representative flow cytometry profiles (*J* and *N*) and quantitative analysis (*K*–*M* and *O*) of total macrophages ($CD45^+CD11b^+F4/80^+$), M1 subsets ($CD86^+CD206^-$), M2 subsets ($CD206^+$), and Tregs ($CD4^+CD25^+FoxP3^+$) in colon tissue ($n = 6$). Data are presented as means ± SD. The Shapiro–Wilk test was employed to assess the normal distribution of the data. Statistical differences among groups were identified by one-way ANOVA, followed by Tukey's multiple comparison tests. $^*P < 0.05$, $^{**}P < 0.01$, $^{***}P < 0.005$, and $^{****}P < 0.0001$; ns denotes no significant difference.

upregulated inflammatory response pathway in IBMSCs showed a contrary downregulation in HMSCs. Specifically, IFN-γ elevated the inflammatory profile of BMSCs, whereas HMSCs, nurtured within an inflammatory niche, manifested lower levels of inflammation. These results indicate that the in vivo activation, differing from the in vitro inflammatory cytokine

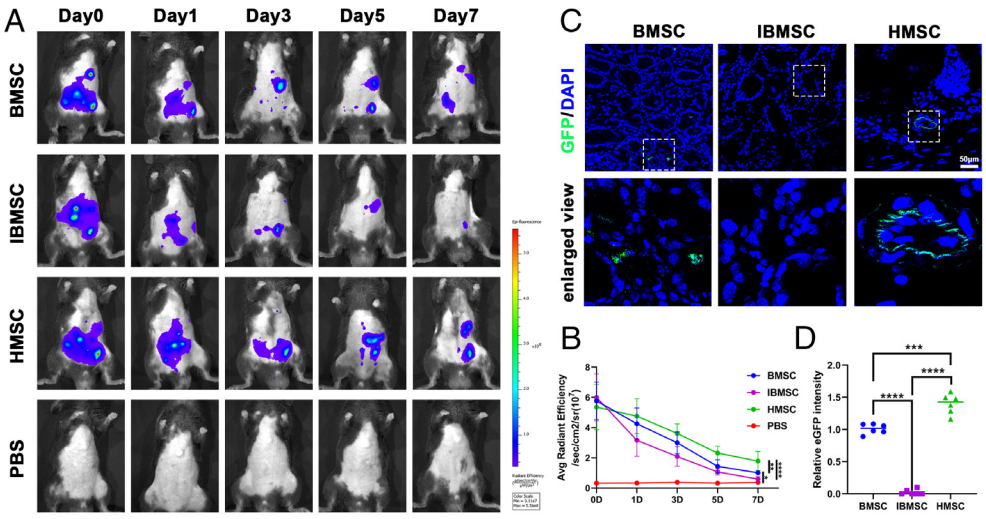

Fig. 6. Persistence of HMSCs after intraperitoneal administration. (*A* and *B*) Representative images (*A*) and quantitative analysis (*B*) from in vivo fluorescent imaging of mice injected with eGFP-MSCs ($n = 5$). (*C* and *D*) Representative immunostainings (*C*) and the quantifications (*D*) of MSC survival (GFP, green). Cell nuclei were counterstained with DAPI (blue). [Scale bar, 50 μm ($n = 6$).] Data are presented as means ± SD. The Shapiro–Wilk test was employed to assess the normal distribution of the data. Statistical differences among groups were identified by one-way ANOVA, followed by Tukey's multiple comparison tests. $^{*}P < 0.05$, $^{**}P < 0.01$, $^{***}P < 0.005$, and $^{****}P < 0.0001$; ns denotes no significant difference.

treatment, endows HMSCs with potent immunomodulatory function without enhancing their intrinsic inflammatory state. Moreover, the physiological state of HMSCs from early-stage developing osteo-organoids is closer to embryonic cells with a lower cellular inflammation level, as evidenced by downregulated senescence-related pathways "Apoptosis" and "p53 signaling pathway," and SASP signaling pathways "TNF signaling pathway" and "NF-kappa B signaling pathway" (*SI Appendix*, Fig. S10*J*). Consistently, our previous work showed that MSCs obtained from osteo-organoids appeared younger compared to BMSCs derived from the same mouse (62).

In addition, we discovered that the in vivo licensing within osteo-organoids conferred two significant advantages in activating MSC immunomodulation function compared to in vitro inflammatory factors treatments. First, HMSCs retained low immunogenicity, a crucial aspect in cell therapy. HMSCs from early-stage developing osteo-organoids exhibited a similar spatiotemporal distribution with trophoblast cells, which prevent maternal rejection by inhibiting Ciita expression (63–65). This may account for the lower levels of MHC-II in HMSCs following IFN-γ treatment, enhancing their ability to evade immune surveillance in pathological conditions. Second, the in vivo activation mode has a lasting impact on HMSCs, contrasting with the transient activation observed in IBMSCs. DNA methylation profiling revealed that the methylation status of PGE2 synthesis–related genes in HMSCs is altered to maintain their active state, while IFN treatment does not affect the methylation levels in BMSCs. This suggests that HMSCs, with their epigenetic memory of immunomodulatory, may exhibit enhanced efficacy in disease treatment.

Inflammatory bowel disease (IBD) includes ulcerative colitis (UC) and Crohn's disease, with UC characterized by severe symptoms such as diarrhea and rectal bleeding (66). Numerous studies indicate that MSCs provide a safe and effective treatment for IBD, overcoming drug resistance, reducing the need for corticosteroids, and minimizing complications. H. Fan et al. demonstrated that IL-1β enhances MSC secretion of immunoregulatory factors and upregulates CXCR4, improving MSC migration to the colon (67). Y. Shi et al. found that MSCs activated by TNF-α in DSS-induced IBD mice exhibit anti-inflammatory properties through the IDO–TSG-6 axis (68). Additionally, hypoxic conditions can enhance MSC therapeutic efficacy in ulcerative colitis by increasing Inos expression (69). To accentuate differences among treatment groups, we increased the DSS concentration, leading to more extensive colonic damage. The in vivo activation approach effectively optimizes MSCs, allowing HMSCs to achieve superior therapeutic outcomes. Furthermore, HMSCs offer advantages such as shorter preparation time, ease of acquisition, and on-demand customization, making them promising candidates for autologous stem cell transplantation. This represents a key direction for our future research.

In summary, we have developed a reproducible method to license the immunomodulatory function of MSCs. Utilizing BMP-2 to initiate osteogenic development, we activated mammalian regenerative capabilities, yielding abundant, homogeneous MSCs while preserving donor tissue integrity. HMSCs derived from osteo-organoids not only retained low immunogenicity but also exhibited sustained, superior immunomodulatory properties. The therapeutic efficacy and long-term survival of HMSCs were further validated in murine colitis models. Collectively, these findings suggest that in vivo licensing via the inflammatory niche is a promising strategy to activate the immunomodulatory potential of mesenchymal stem cells, advancing the field of stem cell therapy.

Materials and Methods

Detailed materials and methods are provided in *SI Appendix, Materials and Methods*, including fabrication and characterization of Sca; fluorescent labeling of polysaccharide-based Sca; animal and animal assays; storage modulus measurement; antibodies and staining reagents; histology and immunohistochemistry; immunofluorescence staining; flow cytometry; isolation and culture of mouse MSCs; CFU-F assay and multilineage differentiation assays; isolation and in vitro polarization of mouse macrophages; isolation of lymphocytes and $CD4^+$ T cells; coculture of MSCs and macrophages; coculture of MSCs with $CD4^+$ T cells; RNA analysis by q-PCR; RNA sequencing and analysis; RRBS; Western blot analysis; In vivo transplantation of MSCs in an experimental colitis model; cytokine measurement; and in vivo fluorescence imaging and statistical analysis. All surgical procedures were approved by the Institutional Animal Care and Use Committee of East China University of Science and Technology.

Data, Materials, and Software Availability. All study data are included in the article and/or *SI Appendix*.

ACKNOWLEDGMENTS. This research was supported by the Basic Science Center Program of National Natural Science Foundation of China (No. T2288102), the Key Program of the National Natural Science Foundation of China (No. 32230059), the National Natural Science Foundation of China (No. 32471406), the Foundation of Frontiers Science Center for Materiobiology and Dynamic Chemistry (JKVD1211002), and the Young Scientists Fund of the National Natural Science Foundation of China (No. 32401128).

Author affiliations: [a]The State Key Laboratory of Bioreactor Engineering, East China University of Science and Technology, Shanghai 200237, People's Republic of China; [b]School of Materials Science and Engineering, Engineering Research Center for Biomedical Materials of the Ministry of Education, East China University of Science and Technology, Shanghai 200237, People's Republic of China; [c]Frontiers Science Center for Materiobiology and Dynamic Chemistry, East China University of Science and Technology, Shanghai 200237, People's Republic of China; and [d]School of Materials Science and Engineering, Key Laboratory for Ultrafine Materials of Ministry of Education, East China University of Science and Technology, Shanghai 200237, People's Republic of China

1. Y. Shi *et al.*, Immunoregulatory mechanisms of mesenchymal stem and stromal cells in inflammatory diseases. *Nat. Rev. Nephrol.* **14**, 493–507 (2018).
2. X. Wu *et al.*, Mesenchymal stromal cell therapies: Immunomodulatory properties and clinical progress. *Stem Cell Res. Ther.* **11**, 1–16 (2020).
3. M. F. Pittenger *et al.*, Mesenchymal stem cell perspective: Cell biology to clinical progress. *NPJ Regen. Med.* **4**, 22 (2019).
4. G. Ren *et al.*, Mesenchymal stem cell-mediated immunosuppression occurs via concerted action of chemokines and nitric oxide. *Cell Stem Cell* **2**, 141–150 (2008).
5. L. Sun *et al.*, Mesenchymal stem cell transplantation reverses multiorgan dysfunction in systemic lupus erythematosus mice and humans. *Stem Cells* **27**, 1421–1432 (2009).
6. L. A. Ortiz *et al.*, Interleukin 1 receptor antagonist mediates the antiinflammatory and antifibrotic effect of mesenchymal stem cells during lung injury. *Proc. Natl. Acad. Sci. U.S.A.* **104**, 11002–11007 (2007).
7. J. Panés *et al.*, Expanded allogeneic adipose-derived mesenchymal stem cells (Cx601) for complex perianal fi stulas in Crohn's disease: A phase 3 randomised, double-blind controlled trial. *Lancet* **38**, 1281–1290 (2016).
8. J. S. Duffield *et al.*, Restoration of tubular epithelial cells during repair of the postischemic kidney occurs independently of bone marrow–Derived stem cells. *J. Clin. Invest.* **115**, 1743–1755 (2005).
9. Y. Wang, X. Chen, W. Cao, Y. Shi, Plasticity of mesenchymal stem cells in immunomodulation: Pathological and therapeutic implications. *Nat. Immunol.* **15**, 1009–1016 (2014).
10. M. J. Murphy, F. P. Barry, Cell contact, prostaglandin E 2 and transforming growth factor beta 1 play non-redundant roles in human mesenchymal stem cell induction of CD4+ CD25High forkhead box P3+ regulatory T cells. *Clin. Exp. Immunol.* **156**, 149–160 (2009).
11. M. Benkhoucha, Hepatocyte growth factor limits autoimmune neuroin ammation via glucocorticoid-induced leucine zipper expression in dendritic cells. *J. Immunol.* **193**, 2743–2752 (2014).
12. T. J. Bartosh *et al.*, Aggregation of human mesenchymal stromal cells (MSCs) into 3D spheroids enhances their antiinflammatory properties. *Proc. Natl. Acad. Sci. U.S.A.* **107**, 13724–13729 (2010).
13. H. Choi, R. H. Lee, N. Bazhanov, J. Y. Oh, D. J. Prockop, Anti-inflammatory protein TSG-6 secreted by activated MSCs attenuates zymosan-induced mouse peritonitis by decreasing TLR2/NF-κB signaling in resident macrophages. *Blood* **118**, 330–338 (2011).
14. A. Hüttmann, C. L. Li, U. Dührsen, Bone marrow-derived stem cells and "plasticity". *Ann. Hematol.* **82**, 599–604 (2003).
15. V. Tisato, K. Naresh, J. Girdlestone, C. Navarrete, F. Dazzi, Mesenchymal stem cells of cord blood origin are effective at preventing but not treating graft-versus-host disease. *Leukemia* **21**, 1992–1999 (2007).
16. E. Zappia *et al.*, Mesenchymal stem cells ameliorate experimental autoimmune encephalomyelitis inducing T-cell anergy. *Blood* **106**, 1755–1761 (2005).
17. K. English, F. P. Barry, C. P. Field-Corbett, B. P. Mahon, IFN-γ and TNF-α differentially regulate immunomodulation by murine mesenchymal stem cells. *Immunol. Lett.* **110**, 91–100 (2007).
18. G. Ren *et al.*, Species variation in the species variation in the mechanisms of mesenchymal stem cell- mediated immunosuppression. *Stem Cells* **27**, 1954–1962 (2009).
19. W. K. Chan *et al.*, MHC expression kinetics and immunogenicity of mesenchymal stromal cells after short-term IFN-γ challenge. *Exp. Hematol.* **36**, 1545–1555 (2008).
20. J. L. Chan *et al.*, Antigen-presenting property of mesenchymal stem cells occurs during a narrow window at low levels of interferon-γ. *Blood* **107**, 4817–4824 (2006).
21. M. Krampera *et al.*, Role for interferon-γ in the immunomodulatory activity of human bone marrow mesenchymal stem cells. *Stem Cells* **24**, 386–398 (2006).
22. P. Jin *et al.*, Interferon- γ and tumor necrosis factor- α polarize bone marrow stromal cells uniformly to a Th1 phenotype. *Sci. Rep.* **6**, 1–11 (2016).
23. K. Dai *et al.*, A BMP-2–triggered in vivo osteo-organoid for cell therapy. *Sci. Adv.* **9**, 1–16 (2023).
24. J. Xu *et al.*, The personalized application of biomaterials based on age and sexuality specific immune responses. *Biomaterials* **278**, 121177 (2021).
25. K. N. Sivanathan, S. Gronthos, Interferon-gamma modification of mesenchymal stem cells: Implications of autologous and allogeneic mesenchymal stem cell therapy in allotransplantation. *Stem Cell Rev. Rep.* **10**, 351–375 (2014).
26. M. Kloc, A. Uosef, M. Leśniak, J. Z. Kubiak, R. M. Ghobrial, Reciprocal interactions between mesenchymal stem cells and macrophages. *Int. J. Dev. Biol.* **64**, 465–469 (2020).
27. J. Li, X. Jiang, H. Li, M. Gelinsky, Z. Gu, Tailoring materials for modulation of macrophage fate. *Adv. Mater.* **33**, 1–38 (2021).
28. E. Kolaczkowska, P. Kubes, Neutrophil recruitment and function. *Nat. Rev. Immunol.* **13**, 159–175 (2013).
29. C. N. Serhan, J. Savill, Resolution of inflammation: The beginning programs the end. *Nat. Immunol.* **6**, 1191–1197 (2005).
30. T. Hu, Z. Luo, K. Li, S. Wang, D. Wu, Zanthoxylum nitidum extract attenuates BMP-2-induced inflammation and hyperpermeability. *Biosci. Rep.* **40**, 1–13 (2020).
31. H. Y. Kim *et al.*, Development of porous beads to provide regulated BMP-2 stimulation for varying durations: In vitro and in vivo studies for bone regeneration. *Biomacromolecules*, 1633–1642 (2016).
32. S. Deng, F. Zhu, K. Dai, J. Wang, C. Liu, Harvest of functional mesenchymal stem cells derived from in vivo osteo-organoids. *Biomater. Transl.* **4**, 270–279 (2023).
33. Q. Z. Zhang *et al.*, Human gingiva-derived mesenchymal stem cells elicit polarization of M2 macrophages and enhance cutaneous wound healing. *Stem Cells* **28**, 1856–1868 (2010).
34. J. Zhang, Y. Rong, C. Luo, W. Cui, Bone marrow mesenchymal stem cell-derived exosomes prevent osteoarthritis by regulating synovial macrophage polarization. *Aging (Albany NY)* **12**, 25138–25152 (2020).
35. B. O. Zhou, R. Yue, M. M. Murphy, J. G. Peyer, S. J. Morrison, Leptin-receptor-expressing mesenchymal stromal cells represent the main source of bone formed by adult bone marrow. *Cell Stem Cell* **15**, 154–168 (2014).
36. S. Morikawa *et al.*, Prospective identification, isolation, and systemic transplantation of multipotent mesenchymal stem cells in murine bone marrow. *J. Exp. Med.* **206**, 2483–2496 (2009).
37. M. B. Herrera *et al.*, Exogenous mesenchymal stem cells localize to the kidney by means of CD44 following acute tubular injury. *Kidney Int.* **72**, 430–441 (2007).
38. A. J. Engler, S. Sen, H. L. Sweeney, D. E. Discher, Matrix elasticity directs stem cell lineage specification. *Cell* **126**, 677–689 (2006).
39. X. Zhang *et al.*, Harnessing matrix stiffness to engineer a bone marrow niche for hematopoietic stem cell rejuvenation. *Cell Stem Cell* **30**, 378–395.e8 (2023).
40. L. R. Amir, D. F. Suniarti, S. Utami, B. Abbas, Chitosan as a potential osteogenic factor compared with dexamethasone in cultured macaque dental pulp stromal cells. *Cell Tissue Res.* **358**, 407–415 (2014).
41. J. D. S. Antonio, R. S. Tuan, Chondrogenesis of limb bud mesenchyme in vitro: Stimulation by cations. *Dev. Biol.* **115**, 313–324 (1986).
42. X. Cao *et al.*, IGF-1C hydrogel improves the therapeutic effects of MSCs on colitis in mice through PGE2–mediated M2 macrophage polarization. *Theranostics* **10**, 7697–7709 (2020).
43. K. Németh *et al.*, Bone marrow stromal cells attenuate sepsis via prostaglandin E 2–dependent reprogramming of host macrophages to increase their interleukin–10 production. *Nat. Med.* **15**, 42–49 (2009).
44. Q. Wang *et al.*, Fra-1 protooncogene regulates IL-6 expression in macrophages and promotes the generation of M2d macrophages. *Cell Res.* **20**, 701–712 (2010).
45. Y. Yue *et al.*, M2b macrophages reduce early reperfusion injury after myocardial ischemia in mice: A predominant role of inhibiting apoptosis via A20. *Int. J. Cardiol.* **245**, 228–235 (2017).
46. D. Philipp, L. Suhr, T. Wahlers, Y. H. Choi, A. Paunel-Görgülü, Preconditioning of bone marrow-derived mesenchymal stem cells highly strengthens their potential to promote IL-6-dependent M2b polarization. *Stem Cell Res. Ther.* **9**, 1–17 (2018).
47. M. Knippenberg, M. N. Helder, B. Zandieh Doulabi, P. I. J. M. Wuisman, J. Klein-Nulend, Osteogenesis versus chondrogenesis by BMP-2 and BMP-7 in adipose stem cells. *Biochem. Biophys. Res. Commun.* **342**, 902–908 (2006).
48. K. L. Wright, J. P. Y. Ting, Epigenetic regulation of MHC-II and CIITA genes. *Trends Immunol.* **27**, 405–412 (2006).
49. P. J. van den Elsen *et al.*, Lack of CIITA expression is central to the absence of antigen presentation functions of trophoblast cells and is caused by methylation of the IFN-γ inducible promoter (PIV) of CIITA. *Hum. Immunol.* **61**, 862 (2020).
50. A. Gonzalez-Pujana *et al.*, Multifunctional biomimetic hydrogel systems to boost the immunomodulatory potential of mesenchymal stromal cells. *Biomaterials* **257**, 120266 (2020).
51. L. D. Moore, T. Le, G. Fan, DNA methylation and its basic function. *Neuropsychopharmacology* **38**, 23–38 (2013).
52. A. Bird, DNA methylation patterns and epigenetic memory. *Genes Dev.* **16**, 6–21 (2002).
53. C. Carli, C. N. Metz, Y. Al-Abed, P. H. Naccache, A. Akoum, Up-regulation of cyclooxygenase-2 expression and prostaglandin E 2 production in human endometriotic cells by macrophage migration inhibitory factor: Involvement of novel kinase signaling pathways. *Endocrinology* **150**, 3128–3137 (2009).
54. A. Jungbauer, S. Medjakovic, Anti-inflammatory properties of culinary herbs and spices that ameliorate the effects of metabolic syndrome. *Maturitas* **71**, 227–239 (2012).
55. A. Berhan *et al.*, Cellular microenvironment stiffness regulates eicosanoid production and signaling pathways. *Am. J. Respir. Cell Mol. Biol.* **63**, 819–830 (2020).
56. G. Feng *et al.*, Protective effect of biogenic polyphosphate nanoparticles from: Synechococcus sp. PCC 7002 on dextran sodium sulphate-induced colitis in mice. *Food Funct.* **10**, 1007–1016 (2019).
57. Y. Zhou, T. Tsai, W. Li, Strategies to retain properties of bone marrow-derived mesenchymal stem cells ex vivo. *Ann. N. Y. Acad. Sci.* **1409**, 3–17 (2017).
58. Y. Li, Y. Xiao, C. Liu, The horizon of materiobiology: A perspective on material-guided cell behaviors and tissue engineering. *Chem. Rev.* **117**, 4376–4421 (2017).
59. H. S. Kim *et al.*, Human umbilical cord blood mesenchymal stem cells reduce colitis in mice by activating NOD2 signaling to COX2. *Gastroenterology* **145**, 1392–1403.e8 (2013).
60. M. Pourjafar *et al.*, All-trans retinoic acid preconditioning enhances proliferation, angiogenesis and migration of mesenchymal stem cell in vitro and enhances wound repair in vivo. *Cell Prolif.* **50**, 1–11 (2017).
61. B. Wang *et al.*, MTOR inhibition improves the immunomodulatory properties of human bone marrow mesenchymal stem cells by inducing COX-2 and PGE2. *Stem Cell Res. Ther.* **8**, 1–13 (2017).
62. K. Dai *et al.*, Generation of rhBMP-2-induced juvenile ossicles in aged mice. *Biomaterials* **258**, 120284 (2020).
63. R. Einenkel, J. Ehrhardt, M. Zygmunt, D. O. Muzzio, Oxygen regulates ILC3 antigen presentation potential and pregnancy-related hormone actions. *Reprod. Biol. Endocrinol.* **20**, 1–9 (2022).
64. S. P. Murphy, T. B. Tomasi, Absence of MHC class II antigen expression in trophoblast cells results from a lack of class II transactivator (CIITA) gene expression. *Mol. Reprod. Dev.* **51**, 1–12 (1998).
65. R. Mattsson, The non-expression of MHC class I1 in trophoblast-cells. *Am. J. Reprod. Immunol.* **40**, 383–384 (1998).
66. H. Huldani *et al.*, Immunotherapy of inflammatory bowel disease (IBD) through mesenchymal stem cells. *Int. Immunopharmacol.* **107**, 108698 (2022).
67. H. Fan *et al.*, Pre-treatment with IL-1β enhances the efficacy of MSC transplantation in DSS-induced colitis. *Cell. Mol. Immunol.* **9**, 473–481 (2012).
68. S. Zhang *et al.*, Inflammatory cytokines-stimulated human muscle stem cells ameliorate ulcerative colitis via the IDO-TSG6 axis. *Stem Cell Res. Ther.* **12**, 1–14 (2021).
69. J. Ying, Q. You, Z. Wang, Z. Hu, Research in veterinary science hypoxic preconditioning promotes the immunosuppressive effects of mesenchymal stem cells in mice with colitis. *Res. Vet. Sci.* **144**, 157–163 (2022).